Millimeter Wave Channel Model for 5G Communication Systems

Chin-Kuo Jao, and Kuan-Hung Chou

***Abstract*—5G communication is likely to be deployed in high frequency band (e.g., 28 GHz). An accurate channel model is necessary to evaluate system performance at initial design phase. However, the valid frequency of 3D SCM channel models developed in 2014 is 2 – 6 GHz. It is not suitable for millimeter band. In order to solve this problem, a new study item on NR channel model was initiated by 3GPP in 2016. The NR channel model consists of common components and extended components. The common components specify the mathematical model and the algorithms used for channel coefficient generation. The extended components are used to model the physical phenomenon of millimeter frequency band. In this paper, we will introduce the NR channel model. Besides, the channel calibration process will also be described.**

***Index Terms*—5G, Channel model, SCM, Pathloss, Penetration loss, Calibration**

I. Introduction

In order to fulfil the 5G requirements on IMT-2020, the 3rd generation parternership project (3GPP) approved a new study item (SI) on New Radio Access Technology (NR) in March 2016. The NR system focuses on three usage scenarios: enhanced Mobile Broadband (eMBB), massive Machine Type Communications (mMTC) and Ultra-Reliable and Low Latency Communications (URLLC). Although 3GPP had completed a study on 3D SCM channel models in 2014 [2], its applied frequency range is 2 – 6 GHz. A new channel model is necessary for the performance evaluation of higher frequency bands (above 6 GHz). Thus a new study item on NR channel model [3] was initiated by 3GPP in 2016 and a lot of channel measurement results are contributed by industry and academic members.

The design objectives and requirements of NR channel model are as follows:

- Channel model SI should take into account the outcome of RAN-level discussion in the 5G requirement study item.
- Complexity in terms of generating channel coefficients, development complexity and simulation time should be considered.
- Support frequency range up to 6 – 100 GHz.
- Take care of mmW propagation aspects such as blocking and atmosphere attenuation.
- The model should be consistent in space, time and frequency.
- Support large channel bandwidths. (up to 10% of carrier frequency)
- Accommodate UE mobility up to 500 Km/h.
- Support large antenna arrays.

The last five objectives are specific features for millimeter wave characteristics. In the NR channel model, they are considered as add-on components which are described in section 7.6 of TR 38.900 [3]. This paper will give an introduction on common components including large-scale model, antenna model and small-scale model.

Since the channel parameters are closely related to network deployment scenarios. There are three main scenarios of interest considered in NR channel model: the *urban micro scenario* (UMi), the *urban macro scenario* (UMa), and the *indoor scenario*. O2O and O2I are the abbreviations of outdoor-to-outdoor and outdoor-to-indoor respectively. Brief descriptions of these three deployment scenarios are described as follows:

(1) UMi with O2O and O2I: the eNBs of UMi street canyon scenario are mounted below rooftop levels of surrounding buildings. UMi open area is intended to capture real-life scenarios such as a city or station square. The width of the typical open area is in the order of 50 to 100 m (e.g.,Tx height:10m, Rx height: 1.5-2.5 m, ISD: 200m).

(2) UMa with O2O and O2I: This is similar to 3D-UMa scenario, where the eNBs are mounted above rooftop levels of surrounding buildings (e.g., Tx height: 25m, Rx height: 1.5-2.5 m, ISD: 500m).

(3) Indoor: This scenario is intended to capture various typical indoor deployment scenarios, including office environments, and shopping malls. The typical office environment is comprised of open cubicle areas, walled offices, open areas, corridors etc. The eNBs are mounted at a height of 2-3 m either on the ceilings or walls. The shopping malls are often 1-5 stories high and may include an open area (or "atrium") shared by several floors. The eNBs are mounted at a height of approximately 3 m on the walls or ceilings of the corridors and shops (e.g., Tx height: 2-3m, Rx height: 1.5m, area: 500 square meters).

The NR channel model consists of *common components* and *extended components*. The common components consist of pathloss models, scenario-specific parameter sets of UMa, UMi-Street Canyon, Indoor-Office and RMa. The common components specify the mathematical model and the algorithms used for channel coefficient generation. The extended components are used to model the physical phenomenon of

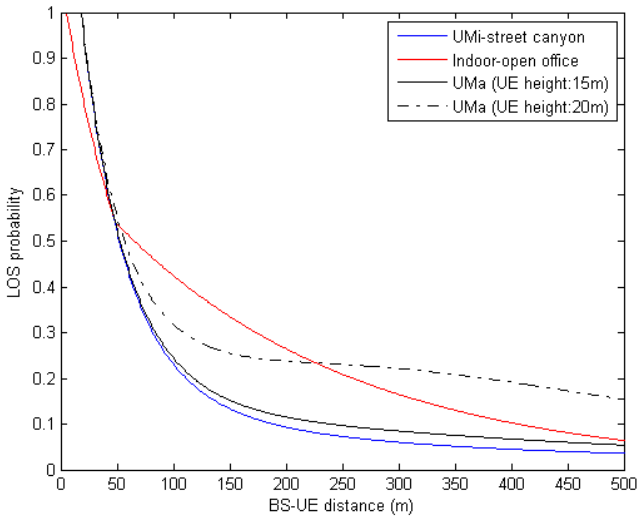

Fig. 1. LOS probability for UMi-street canyon, Indoor-open office, and UMa scenarios.

millimeter frequency band such as oxygen absorption effect, blockage effect, consistencies in time and spatial domain.

Throughout the next sections, we will present the common component parts of NR channel model. Section II presents the large-channel properties. Section III shows antenna array model for MIMO technology. Section IV details the channel coefficients generation procedure. The channel model calibrations are described in Section V for the verification channel modelling methodology between companies.

II. Large-scale Fading Model

The large-scale fading consists of pathloss and penetration loss. Pathloss is the power loss of an electromagnetic wave as it propagates through space. Penetration loss is the signal power loss from an indoor terminal to a base station due to obstruction by a building. The pathloss model is classified as two conditions: line of sight (LOS) and non-line of sight (NLOS). When a user equipment (UE) is dropped in a network, the first step to calculate pathloss is to determine the LOS/NLOS conditions of the UE. If the terminal is an indoor UE, an additional O2I penetration loss should be added.

A. LOS and NLOS Conditions

The LOS/NLOS state condition can be modeled based on ray-tracing simulation results. The BS antenna height settings are 10m for UMi street canyon, 25m for UMa, and 3m for indoor scenarios. Based on the simulation results, a curve fitting method can be applied to get a LOS probability approximation function. The LOS probability function of UMi street canyon is derived as:

$$P_{UMi\_LOS} = \begin{cases} 1 & , d_{2D} \le 18\text{m} \\ \frac{18}{d_{2D}} + \exp\left(-\frac{d_{2D}}{36}\right)\left(1-\frac{18}{d_{2D}}\right) & , 18\text{m} < d_{2D} \end{cases} \quad (1)$$

where d_{2D} is the 2D distance between UE and BS. LOS probability is a distance dependent function. Fig. 1 shows the LOS probability for UMi-street canyon, Indoor-open office, and UMa scenarios. A UE is more likely in LOS state as the UE is closer to a BS. Since the UMa BS with 25m height is higher than other neighbor buildings, the higher UEs will get more LOS probabilities. It should note that the LOS propagation condition is decided on a per-site basis so that a user always experiences identical propagation conditions to all base stations co-located at one site. In other words, the LOS state is site-specific determined. If one site consists of three different directional cells, the UE will experience the same LOS state to the three co-located cells.

B. Pathloss Models

The overall pathloss through propagation link incorporating O-to-I building penetration loss is modelled as:

$$\mathrm{PL} = \mathrm{PL_b} + \mathrm{PL_{tw}} + \mathrm{PL_{in}} + N(0,\sigma_P^2) + N(0,\sigma_{SF}^2) \quad (2)$$

where $\mathrm{PL_b}$ is the basic outdoor path loss given in Table I, $\mathrm{PL_{tw}}$ is the building penetration loss through the external wall, $\mathrm{PL_{in}}$ is the indoor loss dependent on the depth into the building, σ_P is the standard deviation for the penetration loss, and σ_{SF} is the standard deviation for the shadow fading.

In terms of the basic outdoor pathloss $\mathrm{PL_b}$, there are two models considered in the SI meeting. The first one is Close-In (CI) free space reference distance model and the second one is Alpha-Beta-Gamma (ABG) model. Each model has different pros and cons. Finally 3GPP adopts ABG model as the mandatory model for performance evaluation and CI model is optional for reference. The pathloss model shown in Table I is a ABG model. For LOS propagation a dual-slope ABG pathloss model is used which transits from a moderate slope to a steeper slope at distances above a break point distance $\mathrm{d_{BP}}$'. The length of breakpoint distance depends on an environmental height. It can be given by

$$d'_{BP} = 4h'_{BS}h'_{UT}f_c / c, \quad (3)$$

where f_c is the centre frequency in Hz, c is the light speed in free space, and h'_{BS} and h'_{UT} are the effective antenna heights at the BS and the UT, respectively.

It is noted that the pathloss model for 3D channel model [2] can be applied in the frequency range of 2 – 6 GHz for different antenna heights. Now the new pathloss models in Table I are valid for system center frequencies in the range of 0.8 GHz –100 GHz. Fig. 2, Fig. 3 and Fig. 4 are the pathloss degradations for UMi street canyon, UMa and Indoor open office. Fig. 2 ~ Fig. 4 only show the first slope interval since the observed distances are shorter than the break point distances.

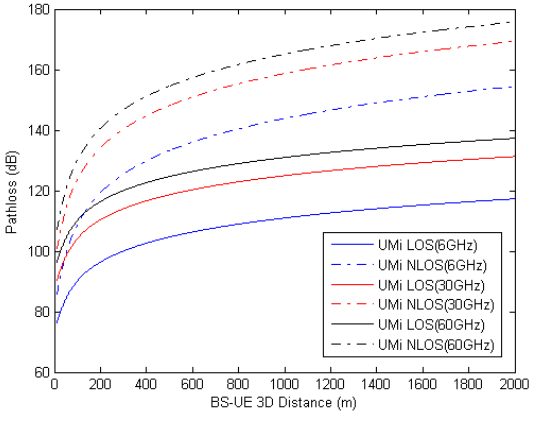

Fig. 2. Pathloss for UMi-street canyon scenario

TABLE I
PATHLOSS MODEL [3]

Scenario	LOS/NLOS	Pathloss PL_b [dB], f_c is in GHz and d is in meters
UMa	LOS	$PL_{\text{UMa-LOS}} = 32.4 + 20\log_{10}(d_{3D}) + 20\log_{10}(f_c)$, $10\text{m} \le d_{2D} \le d'_{BP}$ $PL_{\text{UMa-LOS}} = 32.4 + 40\log_{10}(d_{3D}) + 20\log_{10}(f_c) - 10\log_{10}((d'_{BP})^2 + (h_{BS} - h_{UT})^2)$, $d'_{BP} \le d_{2D} \le 5\text{km}$
	NLOS	$PL_{\text{UMa-NLOS}} = \max(PL_{\text{UMa-LOS}}, PL'_{\text{UMa-NLOS}})$ for $10\text{m} \le d_{2D} \le 5\text{km}$ $PL'_{\text{UMa-NLOS}} = 13.54 + 39.08\log_{10}(d_{3D}) + 20\log_{10}(f_c) - 0.6(h_{UT} - 1.5)$
UMi - Street Canyon	LOS	$PL_{\text{UMi-LOS}} = 32.4 + 21\log_{10}(d_{3D}) + 20\log_{10}(f_c)$, $10\text{m} \le d_{2D} \le d'_{BP}$ $PL_{\text{UMi-LOS}} = 32.4 + 40\log_{10}(d_{3D}) + 20\log_{10}(f_c) - 9.5\log_{10}((d'_{BP})^2 + (h_{BS} - h_{UT})^2)$, $d'_{BP} \le d_{2D} \le 5\text{km}$
	NLOS	$PL_{\text{UMi-NLOS}} = \max(PL_{\text{UMi-LOS}}, PL'_{\text{UMi-NLOS}})$, $10\text{m} \le d_{2D} \le 5\text{km}$ $PL'_{\text{UMi-NLOS}} = 22.4 + 35.3\log_{10}(d_{3D}) + 21.3\log_{10}(f_c) - 0.3(h_{UT} - 1.5)$
InH - Office	LOS	$PL_{\text{InH-LOS}} = 32.4 + 17.3\log_{10}(d_{3D}) + 20\log_{10}(f_c)$
	NLOS	$PL_{\text{InH-NLOS}} = \max(PL_{\text{InH-LOS}}, PL'_{\text{InH-NLOS}})$ $PL'_{\text{InH-NLOS}} = 38.3\log_{10}(d_{3D}) + 17.30 + 24.9\log_{10}(f_c)$

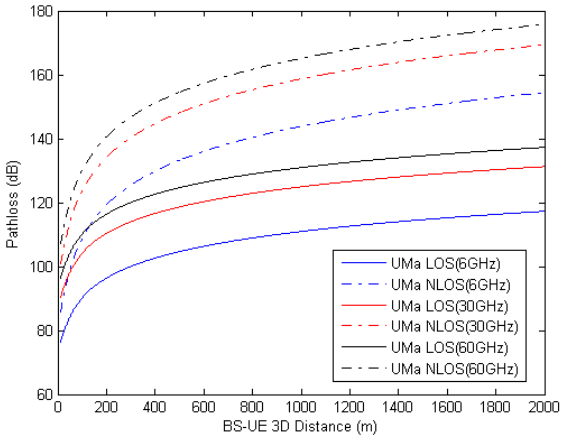

Fig. 3. Pathloss for UMa scenario (UE height = 5m)

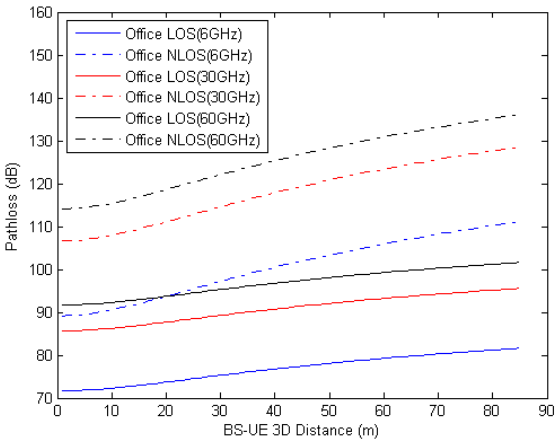

Fig. 4. Pathloss for Indoor open office scenario

The pathloss exponent factor for LOS propagation is about 2, however the factor raises to 3.9 for NLOS UMa and 3.5 for UMi. The pathloss gap between LOS and NLOS is getting wider as the distance increases.

C. *Penetration Loss Models*

In 3D channel model [2], no matter the building is made of concrete or brick, the wall penetration loss PL_{tw} = 20 dB. The new penetration loss model [3] considered various penetration models for different materials including standard glass, IIR glass, concrete, and wood. Based on the measurement results, the penetration loss is frequency dependent, e.g., L_{glass}=2+0.2f, $L_{IIRglass}$=23+0.3f, $L_{concrete}$=5+4f.

The building would not be built with a single material. Thus a composite penetration loss is modeled through a weighted average of the transmission through two different materials. The weight can be given by the relative surface area of each material of the building. Table II provides two typical penetration models: a low loss and a high loss model. Low loss model is based on standard glass and concrete with the ratio of 3/7 and high loss model is based on IIR glass and concrete with the ratio of 7/3. An additional loss of 5 dB was added to the external wall loss to account for non-perpendicular incidence.

The indoor loss PL_{in} is modeled the same as 3D channel model [2] that is $0.5d_{2D\text{-}in}$ dB, where $d_{2D\text{-}in}$ is the indoor distance between UE and the facade of building. Considering the system level simulation assumption, $d_{2D\text{-}in}$ is minimum of two independently generated uniformly distributed variables between 0 and 25 m for RMa, UMa and UMi-Street Canyon. Besides $d_{2D\text{-}in}$ should be UE-specifically generated and applied for all cells.

TABLE II
PENETRATION LOSS MODEL [3]

	Path loss through external wall: PL_{tw} [dB]
Low-loss model	$5-10\log_{10}\left(0.3\cdot 10^{\frac{-L_{glass}}{10}}+0.7\cdot 10^{\frac{-L_{concrete}}{10}}\right)$
High-loss model	$5-10\log_{10}\left(0.7\cdot 10^{\frac{-L_{IIRglass}}{10}}+0.3\cdot 10^{\frac{-L_{concrete}}{10}}\right)$

III. ANTENNA ARRAY MODEL

The 3D channel models support 2D antenna array to perform elevation beamforming via vertical dimension. For 5G channel model, the antenna array model is more generalized from a 2D rectangular array to a panel array with more freedom in the placement of antennas. Fig. 5 illustrates a uniform rectangular panel array comprising $M_g N_g$ panels. M_g is number of panels in a column and N_g is number of panels in a row.

Antenna panels are uniformly spaced in the horizontal direction with a spacing of $d_{g,H}$ and in the vertical direction with a spacing of $d_{g,V}$. On each antenna panel, antenna elements are placed in the vertical and horizontal direction, where N is the number of columns, M is the number of antenna elements with the same polarization in each column. The antenna elements are uniformly spaced in the horizontal direction with a spacing of d_H and in the vertical direction with a spacing of d_V. The antenna panel is either co-polarized (P=1) or cross-polarized (P=2). The rectangular panel array antenna can be described by the following tuple (M_g, N_g, M, N, P).

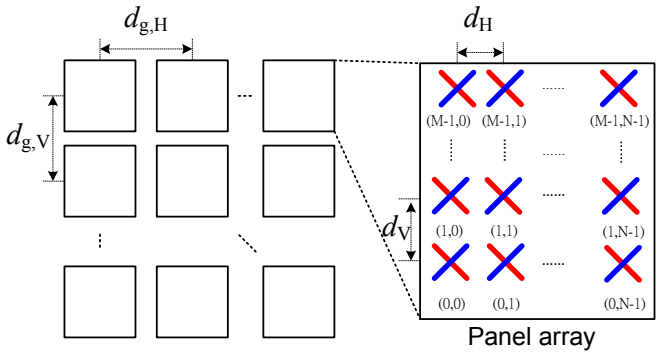

Fig. 5. Antenna array model

A. Antenna Element Pattern

Within the panel antenna array, each antenna element has a directional antenna wide beam pattern to provide horizontal sectorization coverage. In 3GPP, the antenna element pattern is given by:

$$A''(\theta'',\varphi'') = -\min\left\{-\left[A_{E,V}(\theta'')+A_{E,H}(\varphi'')\right], A_m\right\} \quad (4)$$

where

$$A_{E,V}(\theta'') = -\min\left\{12\left(\frac{\theta''-90^\circ}{\theta_{3dB}}\right)^2, SLA_V\right\}, \quad (5)$$

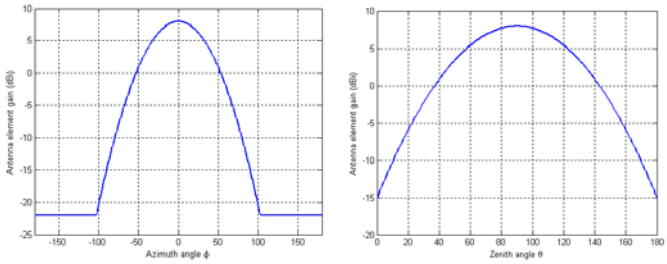

Fig. 6. Gain pattern of antenna element

$$A_{E,H}(\varphi'') = -\min\left\{12\left(\frac{\varphi''}{\varphi_{3dB}}\right)^2, A_m\right\}, \quad (6)$$

$\theta_{3dB} = \varphi_{3dB} = 65^\circ$, $SLA_V = A_m = 30$dB, θ'' and φ'' are the zenith and the azimuth angles in a BS antenna coordinate (local coordinate) respectively. For three-sector cell coverage, each antenna element is designed to have 65 degree horizontal 3dB beam width and vertical beam width is also 65 degree. Fig. 6 depicts the gain pattern of antenna element for both azimuth and zenith angles.

B. TXRU virtualization scheme

A block diagram of MIMO-OFDM system with antenna array is depicted in Fig. 7. One transceiver unit (TXRU) is composed of a digital baseband processor, i.e., IFFT/FFT, and a RF front end circuit. The received signal can be expressed as follows:

$$\mathbf{y} = \mathbf{W}_{TXRU}\mathbf{H}\mathbf{F}_{TXRU}\mathbf{F}_P\mathbf{P}\mathbf{d} + \mathbf{n}, \quad (7)$$

where $\mathbf{F}_{TXRU}$ and $\mathbf{W}_{TXRU}$ are the TXRU virtualization weights on the UE and BS sides respectively. TXRU virtualization weights can be considered as analog beamforming weights between antenna elements and a TXRU. $\mathbf{F}_P$ is the digital antenna port virtualization weight which represents the relation between antenna ports and TXRUs. $\mathbf{P}$ is the conventional digital precoder matrix. It is worth noted that $\mathbf{F}_P$ is an identity matrix before LTE R13 or *CSI-Reporting-Type* is setting to 'CLASS A' in LTE R13. That means the relation of antenna ports and TXRUs are one-to-one mapping.

Fig. 8 shows two typical 1D TXRU architectures considered in TR 36.897 [5]: (1) subarray partition and (2) full-connection. In subarray partition, antenna elements are partitioned into multiple groups of same number of elements. In 1D subarray partition, total M antenna elements in a column are partitioned into M_{TXRU} TXRUs of K elements. Each TXRU is mapped to K antenna elements with the same virtualization weight $\mathbf{F}_{TXRU}$, e.g., 100 degree down-tilt for UMi scenario. The analog TXRU beamforming utilizes coarse direction information and wide RF beams to cover the main rays. The purpose of digital precoding $\mathbf{P}$ is to refine the RF beams to form narrower beams and distinguish multiple multi-path components for beamforming and multiplexing.

In 1D full connection, each TXRU is split into M signals and those M signals are beamformed by a group of M analog phase shifters and variable gain amplifiers. The weighting vectors for

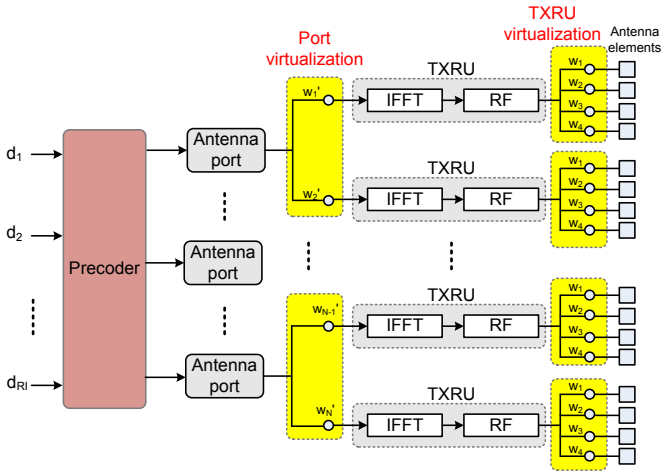

Fig. 7. Antenna array model

each TXRU are different and the M_{TXRU} weighted signals are combined at each antenna element. This structure can produce M_{TXRU} narrow beams, and the function of baseband precoding **P** is to select and apply weights to the narrow beams. Since each TXRU in Alt-1 is implemented with a large number of phase shifters, demultiplexer and multiplexer, the design complexity and hardware cost of the analog front end is very high.

The beam pattern of the antenna array model in Fig. 7 can be classified as: (1) For virtualization weight from TXRU to antenna element, the corresponding beam pattern is called "*TXRU beam pattern*". (2) For digital procoding weight from PDSCH data to TXRU, the corresponding beam pattern is called "*precoding beam pattern*". The final composite beam pattern is composed of precoding beam pattern and TXRU beam pattern.

An illustration of hybrid beamforming pattern with subarray TXRU virtualization is shown in Fig. 9. The antenna configuration is $M = 8$, $M_{\text{TXRU}}=2$, and vertical spacing of $d_V = 0.8\lambda$. A wide TXRU beam pattern is pointing to down-tilt angle 100 degree to cover the main transmission path. Three digital precoding weights (102, 95, and 109 degree) are applied to adjust a narrower beam for capturing the channel cluster information.

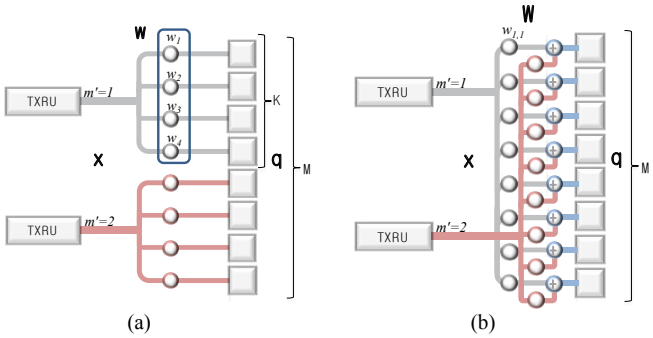

(a) (b)

Fig. 8. (a) 1D subarray TXRU virtualization (b) 1D full-connection TXRU virtualization [5]

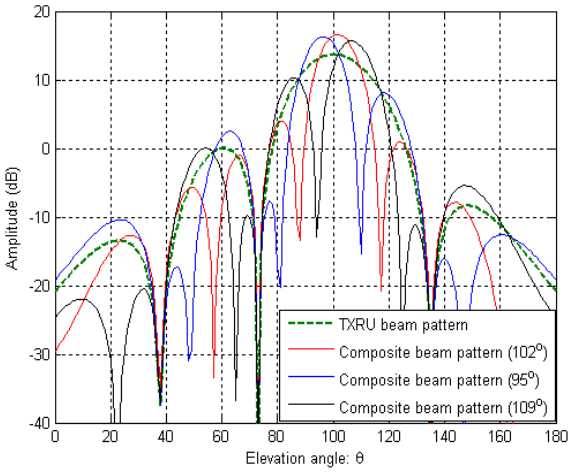

Fig. 9. Composite beam pattern with hybrid beamforming

IV. Channel Model for System Level Simulation

The channel coefficient generation procedure for system level simulation can be described step by step as shown in Fig. 10. There are total 12 steps to elaborate the channel generation process. Steps 1 to 4 are used for generating the large scale states and parameters of each BS-UE link. The large scale states include LOS/NLOS and indoor/outdoor states. The large scale parameters include delay spread (DS), angle spread (AS), Ricean K factor and shadowing fading (SF). These parameters will be applied to generate the small scale parameters in the following steps. Steps 5 to 9 are used for generating the small scale parameters, including delay, cluster power, angle of arrival/departure and XPR, for each propagation link. The small scale parameters will be applied to generate channel coefficients in step 10 to 12.

In the following subsections, we will introduce the process of each step. The detail descriptions of each step are elaborated in 3GPP report TR 38.900 [3].

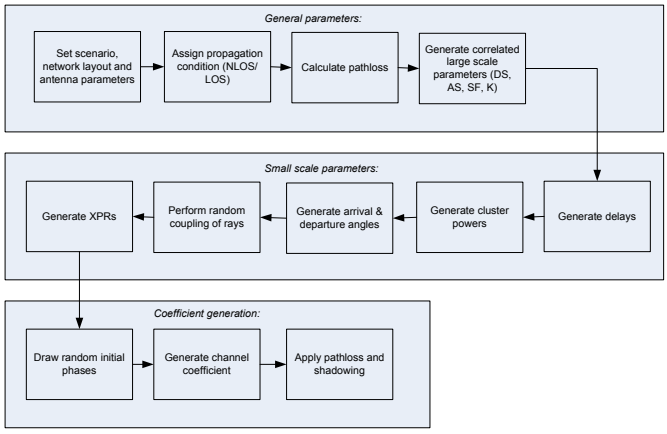

Fig. 10. Channel coefficient generation procedure [3]

A. Large-Scale Parameters Generation

• ***Step 1***: *Set environment, network layout, and antenna array parameters.*

The standard network layout for system level simulation is 19 sites consisting of 57 cells. Then multiple UEs are dropped in the cell with uniform and random manner. The environment is propagation scenario (e.g. UMi-Street Canyon, UMa, or InH-Office).

• ***Step 2***: *Assign LOS/NLOS propagation condition and assign an indoor/outdoor state for each UE.*

The propagation conditions are uncorrelated assigned for different Site-UE links. Also, assign an indoor/outdoor state for each UE. It is noted that all the links from a UE have the same indoor/outdoor state.

• ***Step 3***: *Calculate pathloss with Table I formula.*

The pathloss is generated for each Site-UE link. For eache site, three co-located cells share the same pathloss degradation.

• ***Step 4:*** *Generate correlated large scale parameters for each Site-UE link.*

Total seven correlated large scale parameters should be generated: (1) the RMS delay spread (DS) between the clusters of one link, (2, 3, 4, and 5) the RMS departure/arrival angular spread (i.e., ASD, ASA, ZSD, ZSA), (6) the shadow fading, and (7) the Rician K factor specifying the power ratio between the direct LOS ray and the sum power of all other rays.

After the large scale parameters are created with i.i.d. Gaussian random variables, two correlation processes will be applied. First, a geographic correlation between different links is added based on a specific correlation distance which is listed in Table 7.5-6 in [3]. The correlation process is applied separately for each of the seven large-scale parameters. Second, for each link a cross-correlation between the seven large-scale parameters is established by means of a correlation matrix listing also in Table 7.5-6 in [3].

B. Small-Scale Parameters Generation

After generating the correlated large-scale parameters for each link, the actual small-scale parameters can be determined.

• ***Step 5***: *Generate delays.*

The individual cluster delays τ_n are generated randomly following an exponential distribution.

$$\tau_n' = -r_\tau \mathrm{DS} \ln(X_n) \tag{8}$$

• ***Step 6***: *Generate cluster powers.*

The power contribution P_n of each cluster is derived assuming a single slope exponential power delay profile.

$$P_n' = \exp\left(-\tau_n \frac{r_\tau - 1}{r_\tau \mathrm{DS}}\right) \cdot 10^{\frac{-Z_n}{10}} \tag{9}$$

As shown in Eq. (9), the larger cluster delay leads to weaker cluster power. Within each cluster, the power is distributed uniformly over the 20 rays.

• ***Step 7***: *Generate arrival angles and departure angles for both azimuth and elevation.*

The composite PAS in azimuth of all clusters is modelled as wrapped Gaussian distribution. The AOAs or AODs are determined by applying the inverse Gaussian function with input parameters P_n and RMS angle spread ASA/ASD.

$$\phi_{n,AOA\text{or}\,AOD}' = \frac{2(\text{ASA or ASD}/1.4)\sqrt{-\ln(P_n/\max(P_n))}}{C_\phi} \tag{10}$$

Then, assign positive or negative sign to the angles by multiplying with a random variable X_n with uniform distribution to the discrete set of {1,–1}, and add component $Y_n \sim N(0, (\text{ASA or ASD}/7)^2)$ to introduce random variation:

$$\phi_{n,AOA\text{or}\,AOD} = X_n \phi_{n,AOA\text{or}\,AOD}' + Y_n + \phi_{LOS,AOA\text{or}\,AOD} \tag{11}$$

The generation of ZOA/ZOD follows similar procedures as AOA/AOD except the slightly differences on Laplacian distribution and ZOD offset. The detail description can be referred to [3].

• ***Step 8***: *Coupling of rays within a cluster for both azimuth and elevation.*

Couple randomly AOD/ZOD angles to AOA/ZOA angles within a cluster n, or within a sub-cluster in the case of two strongest clusters. This is to reflect the random scattering effect within a cluster.

• ***Step 9***: *Generate the cross polarization power ratios.*

Generate the cross polarization power ratios (XPR) κ for each ray m of each cluster n as the following equation:

$$\kappa_{n,m} = 10^{X/10} \tag{12}$$

where $X \sim N(\mu_{\mathrm{XPR}}, \sigma_{\mathrm{XPR}}^2)$.

C. Channel Coefficient Generation

• ***Step 10***: *Draw initial random phases.*

Generate random initial phase $\{\Phi_{n,m}^{\theta\theta}, \Phi_{n,m}^{\theta\phi}, \Phi_{n,m}^{\phi\theta}, \Phi_{n,m}^{\phi\phi}\}$ for each ray m of each cluster n and for four different polarization combinations ($\theta\theta$, $\theta\phi$, $\phi\theta$, $\phi\phi$). The distribution for initial phases is uniform within ($-\pi$,π).

• ***Step 11***: *Generate channel coefficients for each cluster n and each receiver and transmitter element pair u, s.*

The computation of the complex path coefficients $h_{u,s,n}$ (t) follows a sum of sinusoids approach that sums over all rays m = 1 . . . M that belong to a cluster n. Eq. (13) shows that the summands for each ray consider the horizontal and vertical polarization components of the UE and BS antenna field patterns, the coupling between departure and arrival rays, the phase offsets between the antenna elements in the MS and BS array, and the time-dependent phase shift resulting from the ray's Doppler component $v_{n,m}$.

$$H_{u,s,n}^{\mathrm{NLOS}}(t)=\sqrt{\frac{P_n}{M}}\sum_{m=1}^{M}\underbrace{\begin{bmatrix}F_{rx,u,\theta}\left(\theta_{n,m,ZOA},\phi_{n,m,AOA}\right)\\F_{rx,u,\phi}\left(\theta_{n,m,ZOA},\phi_{n,m,AOA}\right)\end{bmatrix}^{T}}_{\text{UE antenna pattern}}\underbrace{\begin{bmatrix}\exp\left(j\Phi_{n,m}^{\theta\theta}\right) & \sqrt{\kappa_{n,m}^{-1}}\exp\left(j\Phi_{n,m}^{\theta\phi}\right)\\\sqrt{\kappa_{n,m}^{-1}}\exp\left(j\Phi_{n,m}^{\phi\theta}\right) & \exp\left(j\Phi_{n,m}^{\phi\phi}\right)\end{bmatrix}}_{\text{Coupling between polarization components with random phases}}$$
$$\underbrace{\begin{bmatrix}F_{tx,s,\theta}\left(\theta_{n,m,ZOD},\phi_{n,m,AOD}\right)\\F_{tx,s,\phi}\left(\theta_{n,m,ZOD},\phi_{n,m,AOD}\right)\end{bmatrix}}_{\text{BS antenna pattern}}\underbrace{\exp\left(\frac{j2\pi\left(\hat{r}_{rx,n,m}^{T}.\bar{d}_{rx,u}\right)}{\lambda_0}\right)}_{\text{Phase offset of UE antenna } u}\underbrace{\exp\left(\frac{j2\pi\left(\hat{r}_{tx,n,m}^{T}.\bar{d}_{tx,s}\right)}{\lambda_0}\right)}_{\text{Phase offset of BS antenna } s}\underbrace{\exp\left(j2\pi\frac{\hat{r}_{rx,n,m}^{T}.\bar{v}}{\lambda_0}t\right)}_{\text{Doppler phase shift}} \tag{13}$$

V. Channel Model Calibration

Although the 5G channel model have been developed in TR 38.900 [3]. The implementation of channel model still leave a lot of freedom that could be carried out depends on different implementation methods. For example, the frequency domain granularity do not explicitly addressed in the channel model. So the translation method from channel impulse response to channel frequency response exists various implementation approaches depending on different companies. A lot of detailed models and guidelines sometimes leave room for interpretation. In order to align simulation results between companies, 3GPP usually hold a calibration campaign after the completion of channel model SI.

The calibration campaign for 5G channel model is divided into three phases. The first phase is large scale calibration. At this stage, pathloss, antenna model, and network deployment are the main objects for companies to check whether their channel model is correct. The second phase is full (small scale) calibration. At this stage, all the small scale parameters such cluster delay, AOD, AOA, ZOD, ZOA, etc. should be considered. The third phase is used for additional feature calibration including blockage, spatial consistency model, etc.

The simulation assumptions for full calibration and calibration matrics are list as follows:

- **Scenarios:** 3D-UMa, 3D-UMi-street Canyon, Indoor-office
- **Carrier Frequency:** 6 GHz, 30 GHz, 60GHz, 70GHz
- **Bandwidth:** 20MHz for 6GHz, and 100MHz for 30GHz, 60 GHz and 70 GHz.
- **BS Tx power:** 44 dBm for UMi-Street Canyon, 49dBm for UMa at 6GHz, and 24 dBm for Indoor for all carrier frequencies.
- **BS antenna configurations:**

Config 1: M=4,N=4,P=2, Mg=1, Ng =2, dH = dV = 0.5lambda, $d_{H,g}=d_{V,g}=2.5$

Config 2: Mg=Ng=1, M=N=2, P = 1

- **Calibration metrics:**

(1) Coupling loss

(2) Wideband SIR before receiver without noise

(3) CDF of Delay Spread and Angle Spread (ASD, ZSD, ASA, ZSA) from the serving cell.

(4) CDF of largest (1st) PRB singular values, CDF of smallest (2nd) PRB singular values, and CDF of the ratio between the largest PRB singular value and the smallest PRB singular value.

Antenna configuration 1 should be calibrated with metrics (1), (2) and (3). Antenna configuration 2 should be calibrated with metrics (1), (2) and (4). Fig. 11 to 15 show a part of calibration results. ITRI's calibration data is simulated by ITRI WiSE system level simulator. The detail calibration results are specified in [6].

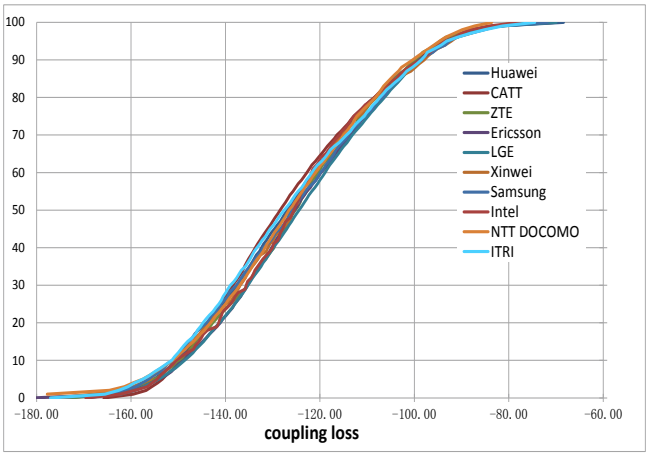

Fig. 11. CDF of coupling loss for 30GHz UMi street canyon with antenna configuration 1.

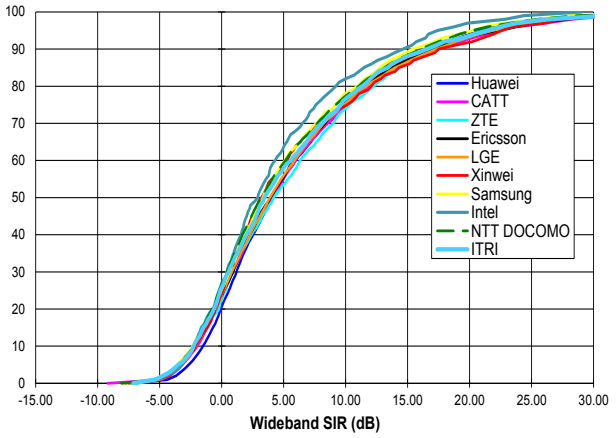

Fig. 12. CDF of wideband SIR for 30GHz UMi street canyon with antenna configuration 1.

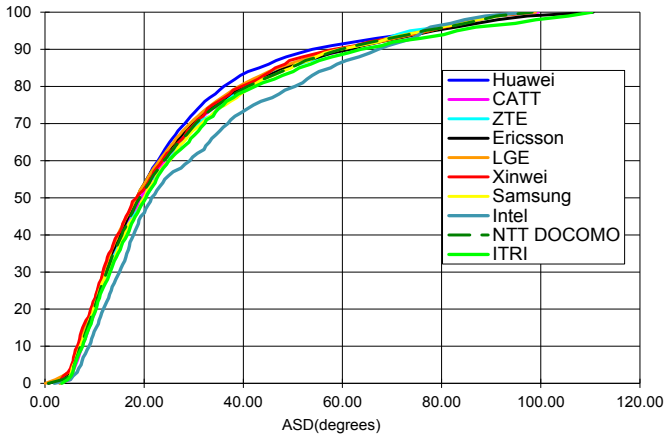

Fig. 13. CDF of azimuth angular spread (ASD) for 30GHz UMi street canyon with antenna configuration 1.

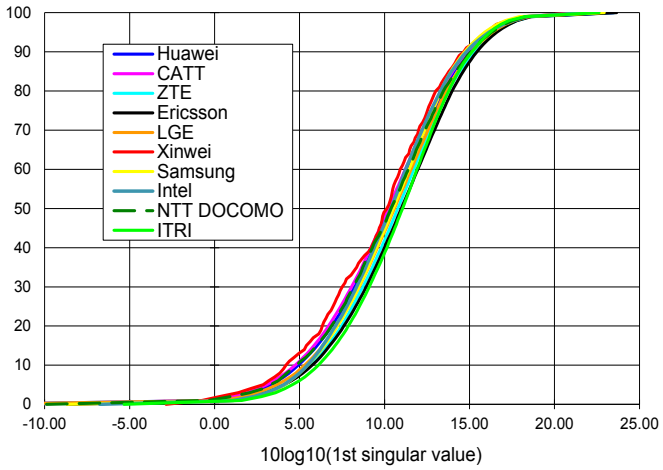

Fig. 14. CDF of largest PRB singular value for 30GHz UMa with antenna configuration 2.

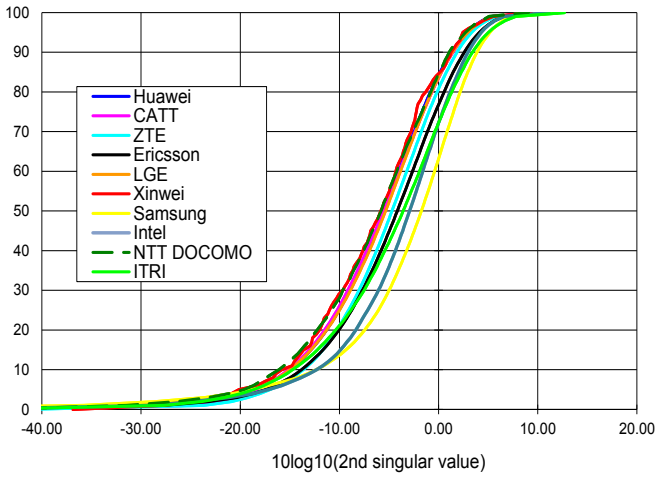

Fig. 15. CDF of smallest PRB singular value for 30GHz UMa with antenna configuration 2.

VI. CONCLUSIONS

In this paper, we introduce millimeter wave channel model for 5G communication system. The channel model is a scenario-specific model which considers three main scenarios for 5G application: UMi – street canyon, UMa, and indoor – open office. The large scale and small scale channel characteristics are elaborated in Section II and IV. The multiple antenna array model is illustrated in Section III. For the alignment of calibration results, we also describe the calibration procedure in Section V.

REFERENCES

[1] 3GPP RP-160671, "New SID Proposal: Study on New Radio Access Technology," March 2016.
[2] 3GPP TR 36.873, "Study on 3D channel model for LTE," September 2014.
[3] 3GPP TR 38.900 v14.1.0, "Channel model for frequency spectrum above 6 GHz," September 2016.
[4] RP-141644, "New SID proposal: study on elevation beamforming/full-Dimension (FD) MIMO for LTE," Samsung, Nokia Networks, 2014.
[5] 3GPP TR 36.897, "Elevation Beamforming/Full-Dimension (FD) MIMO for LTE," June 2015.
[6] R1-167579, "CR for capturing large-scale and full-scale calibration results," Samsung, August 2016.

Chin-Kuo Jao received the Ph.D. degree in electrical engineering from National Central University, Chungli, Taiwan, in 2011. From 2011 to 2013, he was with Sunplus Technology Co., Ltd., where he worked on the DVB-T/T2 baseband receivers. Currently, he is an engineer at the Industrial Technology Research Institute (ITRI), working toward 3GPP LTE-Advanced system and 5G NR system. His research interests include massive MIMO systems, MIMO signal processing, and VLSI design for wireless communications.

Kuan-Hung Chou received the B.S. degree in Information Engineering and Computer Science from Feng Chia University, Taichung, Taiwan in 2005, and received the M.S. and Ph.D. degrees in Computer Science and Engineering from National Chung-Hsing University, Taichung, Taiwan in 2007 and 2011, respectively. He is now a senior engineer in the Information and Communications Research Laboratories, Industrial Technology Research Institute, Taiwan. His research interests include computer networks, wireless networks, optical networks, switching systems and interconnection networks.